

Transient 3-D FEM Computation of Eddy-Current Losses in the Rotor of a Claw-Pole Alternator

Christian Kaehler and Gerhard Henneberger

Abstract—The three-dimensional finite-element method (FEM) allows for the calculation of eddy currents in the claws of synchronous claw-pole alternators taking the rotational geometry movement into account. A transient edge-based vector formulation is utilized to compute the induced eddy-current losses in the rotor caused by the stator slotting. The theory of this formulation is outlined and the FEM model of the alternator is described. On a model built in series-production the local loss distribution on the rotor claw is discussed as well as the speed characteristics of the eddy-current losses. The use of adaptive mesh optimization leads to corrected results which are compared to local temperature measurements.

Index Terms—Adaptive h-refinement, eddy-current losses, rotational geometry movement, transient 3-D FEM computation.

I. INTRODUCTION

THE EFFICIENCY of electric machines is decreased by different loss mechanisms. In the case of the claw-pole alternator, these are dominantly ohmic losses in the coils, that define the loss behavior in the lower speed range of the alternator. Additionally, iron losses, consisting of hysteresis and eddy-current losses, define the high-speed loss characteristics of this machine [1]. Both can be broken down into rotor and stator parts. Whereas the ohmic losses are directly calculated in dependence on the coil currents, an analytic description of the iron losses is not possible due to the geometric complexity of the three-dimensional (3-D) field distribution.

Measurements of the total losses and a subtraction of all analytically defined loss mechanisms lead to a separation of the iron losses. But these separated losses are error-prone due to the long series of measurements.

In order to optimize electric machines efficiently numerical tools for the design process have to be developed. Usage of the finite-element method (FEM) combined with a time-stepping approach allows to calculate the eddy currents in conducting materials which are induced by an alternating magnetic field. In the case of the claw-pole synchronous machine, the eddy-current losses in the rotor claws are caused by the rotor movement in combination with the stator slotting. The magnetic flux pulsates with the slot frequency (e.g., $f_{\text{slot}} = 1800$ Hz at alternator speed $n = 3000$ rpm). The flux pulsations induce the eddy currents in the claws made of massive steel.

In this paper, a transient edge-based FEM approach [2] applied on the alternator is outlined. The 3-D model of the claw-pole alternator is described. The characteristic curve

of the rotor eddy-current losses depending on the alternator speed in generator mode is presented. Adaptive h-refinement in eddy-current regions with two different local error-estimation strategies is applied. The calculation results are then verified by temperature measurements on the rotor claws.

II. THEORY OF THE EDGE-BASED SOLVER

The applied edge-based solver is part of an object-oriented solver package [3]. It utilizes a transient edge-based FEM formulation on simply-connected eddy-current regions taking the rotational movement into account by means of time stepping.

The transient \vec{A} approach applies only the magnetic vector potential \vec{A} in all regions Ω by means of the following equation (in Galerkin formulation) [2]

$$\int_{\Omega} \left(\nabla \times \vec{\alpha}_i \cdot \nu \nabla \times \vec{A}(t) + \sigma \frac{d\vec{A}(t)}{dt} \right) d\Omega = \int_{\Omega} \left(\vec{\alpha}_i \cdot \vec{J}_0(t) + \nabla \times \vec{\alpha}_i \cdot \nu \vec{B}_r(t) \right) d\Omega. \quad (1)$$

The material parameters ν and σ represent the nonlinear reluctance and the linear conductivity, respectively. $\vec{\alpha}_i$ defines the shape function of an edge element (in this solver first-order tetrahedra). $\vec{J}_0(t)$ describes the given coil current density, while $\vec{B}_r(t)$ defines remanence. Note, that external currents ($\vec{J}_0(t) > \vec{0}$) are only allowed in nonconducting regions ($\sigma = 0$) while remanence is valid in all regions ($\sigma \geq 0$).

The time-stepping algorithm interpolates the time-dependent variables linearly

$$\vec{A}(t) = \tau \cdot \vec{A}_{n+1} + (1 - \tau) \vec{A}_n \quad \text{ditto for } \vec{J}_0(t), \vec{B}_r(t);$$

$$\frac{\partial \vec{A}(t)}{\partial t} = \frac{1}{\Delta t} (\vec{A}_{n+1} - \vec{A}_n) \quad (2)$$

where n represents the number of the transient step, Δt the time in between two transient steps and τ the relaxation factor. The relaxation factor in between transient steps is chosen as $\tau = 2/3$ (Galerkin-scheme) [4].

The magnetic flux density \vec{B} and the eddy-current density \vec{J} are computed from the magnetic vector potential as follows:

$$\vec{B} = \nabla \times \vec{A}, \quad \vec{J} = -\sigma \frac{\vec{A}_{n+1} - \vec{A}_n}{\Delta t}. \quad (3)$$

In this approach, no boundary conditions have to be applied on the boundaries between eddy-current and nonconducting regions. Only the usual periodic and Dirichlet conditions for \vec{A} on the model boundaries are used [5].

The resulting global matrix is symmetric, thus allowing the storage as lower or upper triangular matrix and the use of the

Manuscript received July 1, 2003.

The authors are with the Department of Electrical Machines (IEM), Aachen University (RWTH), D-52056 Aachen, Germany. (e-mail: christian.kaehler@iem.rwth-aachen.de)

Digital Object Identifier 10.1109/TMAG.2004.825469

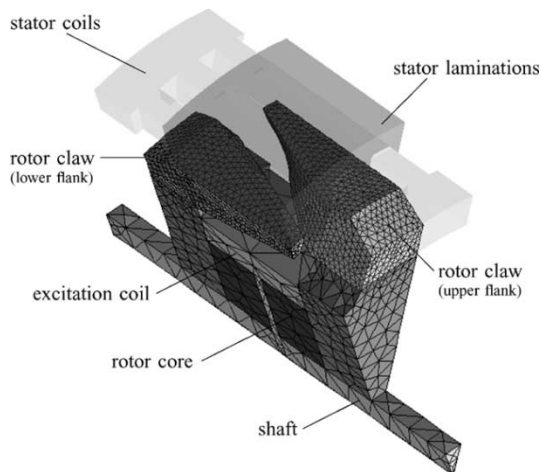


Fig. 1. Model of series-production alternator.

Cholesky-CG combination [2] of the ITL package [6]. Saturation effects are computed with an overlaying Newton–Raphson procedure for each transient step.

To represent rotational movement a lock-step method is utilized. Boundary conditions pair edges in a sliding area mesh. In each step a search function connects the edges of this area depending on the displacement in between the transient steps, while the actual mesh remains stationary [7]. Thus, the flux is coupled between moving and stationary regions.

III. FINITE-ELEMENT MODEL

Only magnetically relevant components of the synchronous claw-pole alternator are modeled. Since the geometry of the alternator is symmetric antiperiodic boundaries and a special geometric regrouping reduce the FEM model to one pole pitch or 30° [8]. Thus, with small calculation time dense meshes can be computed efficiently.

A model of the alternator in production is depicted in Fig. 1 with translucent stator regions. The mesh density of this model with about half an element layer per penetration depth

$$\delta = \frac{1}{\sqrt{\sigma \cdot \mu \cdot f_{\text{slot}} \cdot \pi}} \quad (4)$$

of the eddy currents on the claw surface is rather coarse. Therefore, in order to improve the loss results adaptive h-refinement of the mesh is conducted in all eddy-current regions. The depicted mesh is labeled *starting mesh* in this paper.

The edge-grouping routine of the transient solver described in Section II depends on a special air-gap discretization. To implement the change of geometry, the FEM mesh of the alternator is separated into moving elements in the rotor and stationary elements in the stator. The boundary area of these two meshes is located in the middle of the air gap. It is meshed identically in both separate meshes.

IV. CALCULATIONS AND RESULTS

All calculations are conducted at constant alternator speed. The mechanical step angle amounts to $\alpha = 1^\circ$, leading to for example $\Delta t = 55.556 \mu\text{s}$ in between transient steps at a speed of $n = 3000$ rpm. The excitation current of $I_f = 4$ A is impressed into the rotor DC coil. The three-phase current of the al-

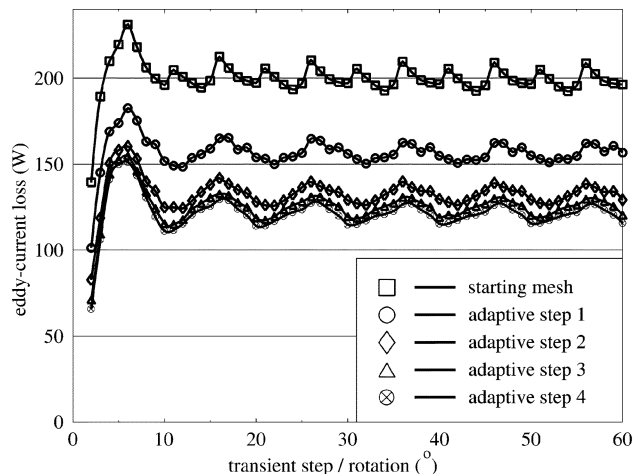


Fig. 2. Eddy-current loss versus transient step.

ternator in generator mode is injected in the stator coils turning synchronously with the rotor. The material conductivity of iron $\sigma = 7.5 \cdot 10^6 [\Omega\text{m}]^{-1}$ at material temperature $T = 75^\circ\text{C}$ is used for the massive steel regions of the claws.

A. Adaptive Mesh Optimization

The computations begin with the coarse starting mesh of about 125 000 first-order elements. In order to calculate the discretization error, the eddy-current density of a full loss period is taken into account by using the arithmetic mean value of the local error for each element. In each adaptive step a given ratio of the elements in eddy-current regions with the highest local error is refined by h-partitioning.

Two strategies for the local error estimation are evaluated. The first strategy defines the highest error in dependence of the gradient of the eddy-current density \vec{J}

$$\varepsilon_1 = |\nabla \cdot \vec{J}|. \quad (5)$$

The second strategy evaluates the error of the joule loss in each element e rated by the total loss of the conducting region [9]

$$\varepsilon_2 = \frac{\int_{\Omega_e} (\vec{J}_e - \vec{J}_{avr}) \cdot \vec{E}_e d\Omega_e}{\int_{\Omega} \vec{J} \cdot \vec{E} d\Omega}. \quad (6)$$

where \vec{J}_e and \vec{E}_e are the eddy-current density and the electric field strength of element e while \vec{J}_{avr} defines the average eddy-current density of all contact elements.

The total eddy-current loss in the claws over the rotation for different adaptive steps with the second error estimator ε_2 is depicted in Fig. 2.

The \vec{A} approach implies an essential static start since otherwise the eddy currents rise dramatically in the first transient step. Without static start step the solver computes the eddy currents that would build up, if the machine started from no excitation and zero speed to full excitation and full speed in one time step. The relaxation time would then prolong to about 100 transient steps. With static start step, the computation simulates the spontaneous change from zero to full conductivity of the claw-pole material. After a short settling time of about 15 time steps, a periodicity of the eddy-current losses of $\Delta\alpha = 10^\circ$ mechanical occurs, as expected for the synchronous machine.

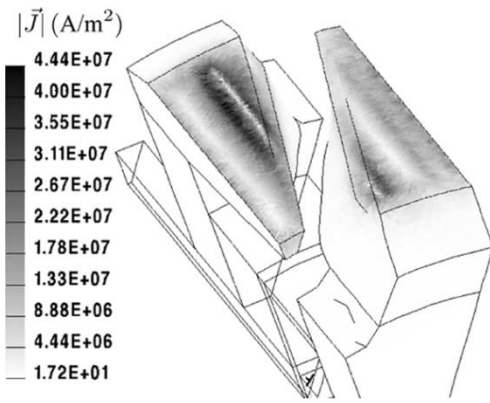


Fig. 3. Eddy-current density at time step 54 and $n = 3000$ rpm.

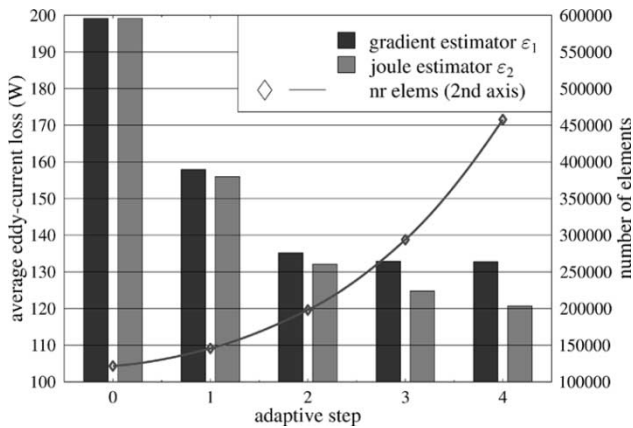


Fig. 4. Eddy-current loss and number of elements versus adaptive step.

The eddy-current distribution for a specific time step at alternator speed $n = 3000$ rpm is depicted in Fig. 3. The maximum eddy-current values as well as the maximum magnetic flux densities are located on the lower flank of the claw (generator effect), with the rotor turning mathematically positive.

With finer meshes the average eddy-current loss decreases (Fig. 4). The adaption ends when the difference of the average loss values before and after a specific adaptive step falls below a given limit of 5%. This limit is reached after 3–4 steps corresponding to 4–8 element layers within the penetration depth δ .

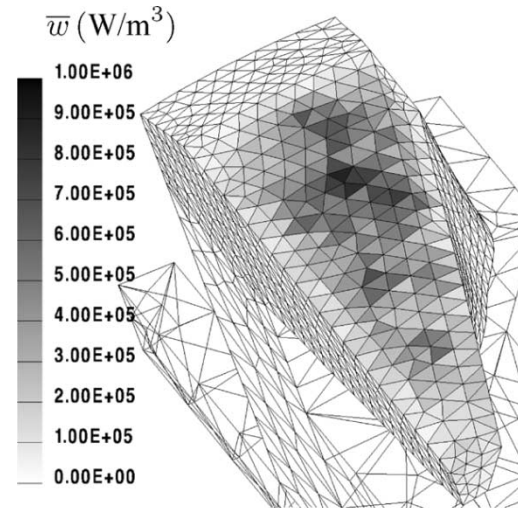
Note, that the second error estimator ε_2 allows for more refinement steps than the gradient estimator ε_1 which stagnates after step 3 in Fig. 4. Therefore, the estimator ε_2 based on the joule loss as defined in (6) leads essentially to smaller discretization errors.

Both error estimators cause mesh refinements on the surface of the rotor claw interfacing the air gap. Fig. 5 depicts the density of the mesh on the claw tip comparing the starting mesh [Fig. 5(a)] to a mesh after three adaptive steps [Fig. 5(b)].

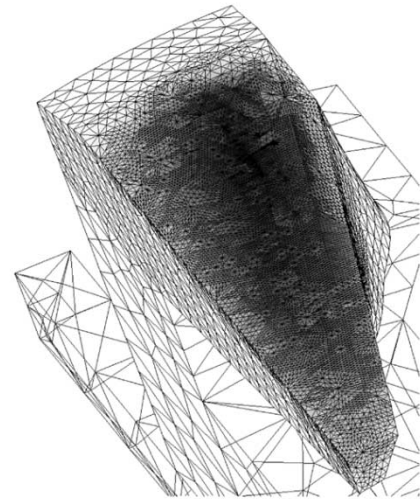
The calculation of the average energy density \bar{w} of the eddy currents over a period of the losses reads

$$\bar{w} = \frac{\Delta t}{\sigma} \cdot \sum_{n=1}^N \vec{J}_n^2 \quad (7)$$

with N being the number of steps in a period and \vec{J}_n the eddy-current density of an element at step n . The resulting average



(a) Loss energy of starting mesh



(b) Loss energy of adaptive step 3

Fig. 5. Average eddy-current loss energy at $n = 6000$ rpm on the lower flank of the rotor claw.

eddy-current energy for $n = 6000$ rpm is depicted in Fig. 5(a) and (b). Again the maximum is located on the lower flank.

The distribution of the average loss energy can later be used as excitation for thermal solvers. Since the thermal distribution will only differ by diffusion effects from the energy distribution, the maxima distribution in Fig. 5(b) has already been compared to hotspot distributions in temperature measurements on the surfaces of the rotor claws showing good conformity.

Fig. 6 depicts such a hot-spot measurement conducted on the alternator by use of thermal paint on the rotor claws. The paint creates an irreversible visual picture of the temperature contour pattern. This pattern resembles the calculated eddy-current energy distribution.

B. Speed Characteristic of Eddy-Current Loss

The working points of the alternator are varied from $n = 1500$ rpm to $n = 10000$ rpm. These computations lead to the characteristic speed curve of the average eddy-current losses in the rotor of the synchronous claw-pole alternator in generator mode on a half-logarithmic scale as presented in Fig. 7. These have already been verified by loss measurements based on the



Fig. 6. Measured temperature contour on the rotor claws.

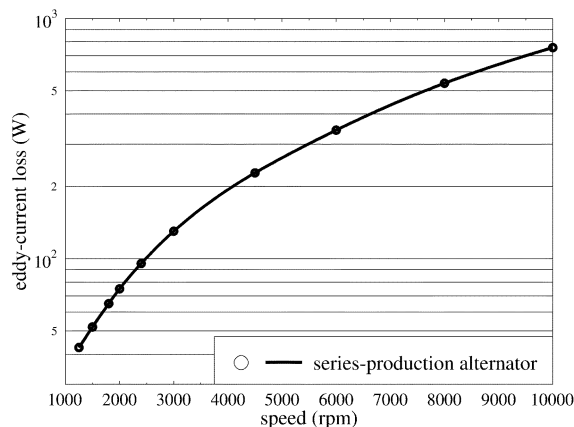


Fig. 7. Eddy-current losses versus alternator speed.

separation of known loss mechanisms proving good conformity [10].

The computed speed characteristic of the eddy-current losses can later be used in steady-state simulations of the alternator and of the entire on-board supply system of the automobile.

V. CONCLUSION

A transient 3-D FEM approach to calculate the eddy currents in the claws of a synchronous claw-pole alternator is applied taking the rotational movement into account. It is exemplified on a series-production alternator. The calculations are conducted in generator mode at constant speed.

Two different error estimators are compared that lead, in combination with adaptive remeshing, to the characteristic speed curve of the eddy-current losses in the rotor. Essentially, the estimator based on the joule loss proves to be better fit for the application due to a higher possible number of h-refinement steps.

The calculated losses fit measurements based on loss separation techniques. Additionally, the eddy-current energy distribution is compared to temperature contours measured by means of thermal paint. The local distributions resemble each other perfectly. Thus the presented transient FEM approach allows for local and global prediction of the eddy-current losses in the rotor of the claw-pole alternator. Furthermore the transient FEM will be utilized for design optimization of future alternator models.

ACKNOWLEDGMENT

All calculations have been utilized on a claw-pole alternator of the Compact Generator Series of the industrial partner Robert Bosch GmbH [11], which has conducted all measurements. For modeling and discretization the commercial program ANSYS Version 7.0 has been used [12]. All geometry, mesh and solution pictures have been generated by the open-source postprocessing tool iMOOSE.trinity [13], [3].

REFERENCES

- [1] K. G. Bürger, H. P. Gröter, H. J. Lutz, F. Meyer, and W. Schleuter, "Generation im Kraftfahrzeug—Stand der Technik und Entwicklungstendenzen," presented at the *Tagung: Nebenaggregate im Fahrzeug*, H. der Technik, Ed., Essen, Germany, Oct. 1994.
- [2] A. Kameari and K. Koganezawa, "Convergence of ICG method in FEM using edge elements without gauge condition," *IEEE Trans. Magn.*, vol. 33, pp. 1223–1226, Mar. 1997.
- [3] G. Ariens, T. Bauer, C. Kaehler, W. Mai, C. Monzel, D. van Riesen, and C. Schlensok. Innovative Modern Object-Oriented Solving Environment—iMOOSE. [Online]. Available: <http://www.imoose.de>
- [4] O. C. Zienkiewicz and R. L. Taylor, *The Finite Element Method*. New York: McGraw-Hill, 1991.
- [5] C. Kaehler, D. van Riesen, D. Albertz, and G. Henneberger, "Comparison of the $\vec{A} - \vec{A}$, \vec{T} - and the \vec{A} -formulation for the computation of transient eddy-current field problems with edge elements," presented at the *10th Int. IGTE Symp. Numerical Field Calculation in Electrical Engineering*, Graz, Austria, Sept. 2002.
- [6] A. Lumsdaine, J. Siek, and L.-Q. Lee. The Iterative Template Library—Itl. [Online]. Available: <http://www.lsc.nd.edu/research/itl>
- [7] C. Kaehler and G. Henneberger, "Eddy-current computation on a one pole-pitch model of a synchronous claw-pole alternator," *COMPEL*, vol. 22, no. 4, pp. 834–846, 2003.
- [8] —, "Eddy current computation in the claws of a synchronous claw pole alternator in generator mode," *IEEE Trans. Magn.*, vol. 38, pp. 1201–1204, Mar. 2002.
- [9] K. Tani, T. Yamada, and Y. Kawase, "Error estimation for transient finite element method using edge elements," *IEEE Trans. Magn.*, vol. 36, pp. 1488–1491, July 2000.
- [10] C. Kaehler, "Numerische Berechnung der Wirbelstromverluste von Drehstrom-Klauenpolgeneratoren," Ph.D. dissertation, Dept. Electrical Machines, Aachen Univ., Aachen, Germany, 2003.
- [11] Robert Bosch GmbH. [Online]. Available: <http://www.bosch.com>
- [12] Ansys Inc.-Open and Flexible Simulation Software Solutions for Every Phase of Product Design. Ansys Inc., Canonsburg, PA. [Online]. Available: <http://www.ansys.com>
- [13] C. Monzel and G. Henneberger, "Object-oriented design of a visualization tool on top of a FEM package," in *Proc. 13th Conf. Computation of Electromagnetic Fields*, vol. 2, Evian, France, July 2001, pp. 216–217.